Supporting Information

Heterogeneous Seeds Boosting the Self-Lithiophilic Host with Dual-Phase Lithium Storage for Stable Lithium-Metal Anode

*Zhicui Song [a,c], Jing Xue [b], Chaohui Wei [c], Donghuang Wang [c], Yingchun Ding [d], Aijun Zhou [a,c], Jingze Li [a,c]**

a School of Materials and Energy, University of Electronic Science and Technology of China, Chengdu 611731, China

b School of Mathematics and Physics, Weinan Normal University, Weinan 714099, China

c Huzhou Key Laboratory of Smart and Clean Energy, Yangtze Delta Region Institute (Huzhou), University of Electronic Science and Technology of China, Huzhou 313001, China

d College of Material and Chemical Engineering, Yibin University, Yibin 644000, China

Corresponding author E-mail: lijingze@uestc.edu.cn (J. Z. Li)

1. Experimental

1.1 Materials and electrodes preparation

Carbon fiber (CF) and polyvinylidene fluoride (PVDF) were mixed in a N-methyl-2-pyrrolidine (NMP) solution with a mass ratio of 9:1. After thoroughly stirred, the as-formed homogeneous slurry was coated onto Cu foil and then placed in a vacuum oven at 80 °C overnight. Subsequently, the CF electrode was obtained by directly punching the film into circular pieces with a diameter of 12 mm. For the fabrication of CF@Pt electrode, an ion sputtering instrument (ETD, 2000C) was employed at 8 mA for 220 s

to ensure a uniform Pt covering on the surface of the CF film.

$LiFePO_4$ (LFP) cathode was also fabricated by a slurry-casted method for full cells testing. Specially, 80 wt% LFP powders, 10 wt% PVDF binder, and 10 wt% Super-P were thoroughly dispersed in NMP solution. Subsequently, Al foil was served as the current collector and the as-obtained slurry was coated. Finally, the LFP cathode was obtained after NMP solvent drying out. The areal loading of the as-fabricated LFP cathode is about 10.5 mg cm^{-2}.

1.2 Electrochemical property characterizations

In this contribution, CR2032-type coin cells were assembled in a glove box filled with Ar to evaluate the electrochemical properties of the as-fabricated electrodes. The electrolyte is 1 M lithium bis(trifluoromethanesulfonyl)imide (LiTFSI) and 2 wt% $LiNO_3$ additives in 1,2-dimethoxyethane (DME) and 1,3-dioxolane (DOL) (v/v = 1:1), while the Celgard 2325 membrane is regarded as the separator. The assembled coin cells were monitored in a Neware battery testing system with a galvanostatic mode. For the Coulombic efficiency test, the half cells were assembled by using the CF@Pt (or Cu foil, or CF) film as the working electrode, and a Li foil served as the counter electrode. A fixed amount of Li was deposited onto the working electrode and then stripped to a cut-off voltage of 1.0 V for each cycle. Specially, the working electrode was activated between 0.01 and 1.0 V vs. Li/Li^+ (5 cycles) at 0.5 mA cm^{-2} to stabilize the SEI film. The corresponding Coulombic efficiency was calculated by the percentage of the dissolution capacity divided by the deposition capacity. The symmetrical cells were respectively tested at a constant current density of 0.5 and 1.0 mA cm^{-2} with a

fixed cut-off capacity of 1.0 mAh cm^{-2}. It should be stated that the electrodes used in symmetrical cells were firstly pre-deposited with 2.5 mAh cm^{-2} of Li. The LFP-based full cells were assessed in the voltage range of 2.5-4.2 V versus Li^+/Li. The Tafel plot measurements were conducted on an electrochemical workstation (CHI660C, Shanghai, Chenhua) with a scan rate of 0.5 mV s^{-1}.

1.3 Material characterizations

The morphologies, microstructures and element distributions of the as-fabricated samples or the cycled electrodes were visualized at 15 kV by field emission scanning electron microscopy (FE-SEM, Hitachi, S3400N) of which is equipped with energy-dispersive X-ray spectroscopy (EDS). Specially, all the Li containing samples were prepared in an Ar-filled glove-box and loaded into a sealed transfer vessel for the followed SEM characterization. The electrodes obtained from the disassembled cells were rinsed with DME solvent and fully dried in the glove-box.

2. Figures and Captions

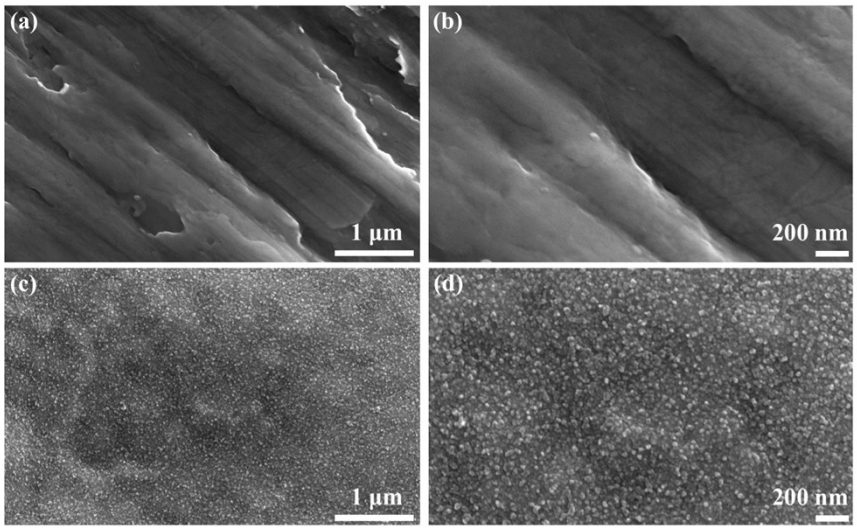

Figure S1. SEM images of (a, b) bare Cu foil and (c, d) Pt-coated bare Cu foil (Cu@Pt).

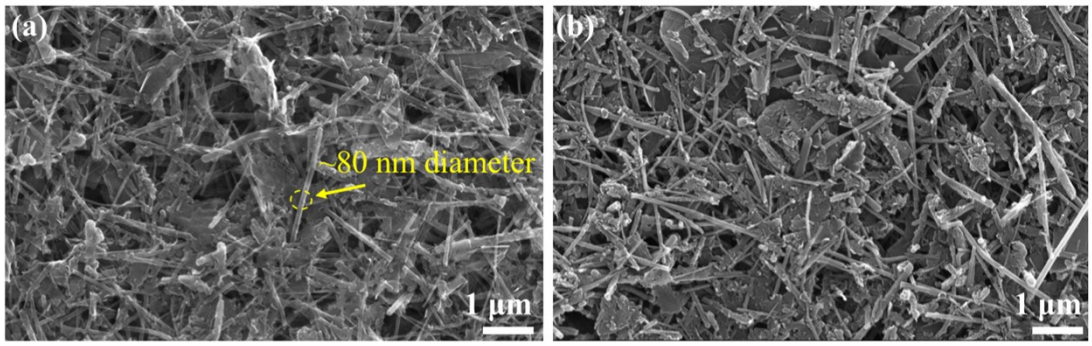

Figure S2. The high magnification SEM images of (e) CF and (f) CF@Pt.

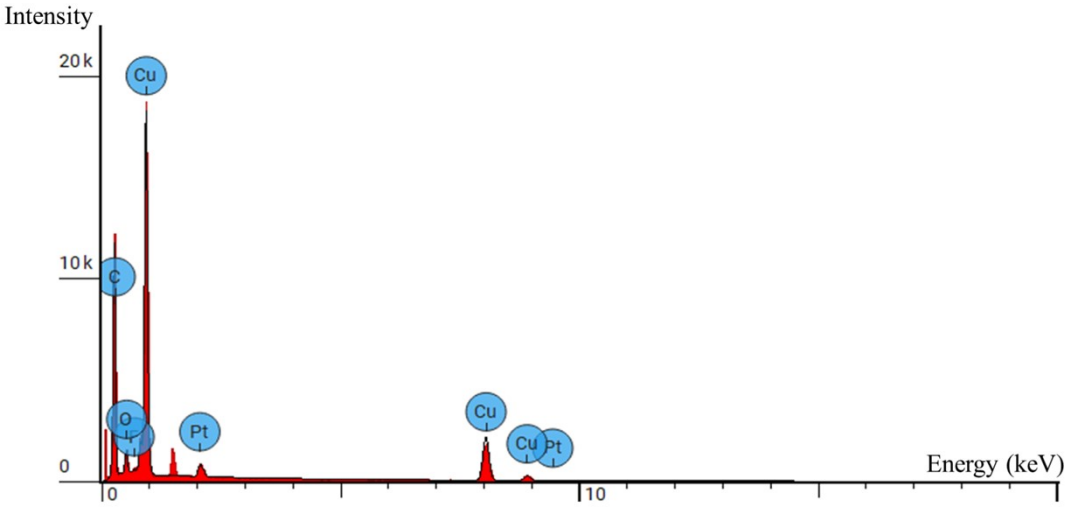

	Element number	Element symbol	Element name	Atomic concentration percentage (%)	Weight concentration percentage (%)
	6	C	Carbon	78.131	43.700
	8	O	Oxygen	4.563	3.400
	9	F	Fluorine	0.226	0.200
	29	Cu	Copper	16.728	49.500
	78	Pt	Platinum	0.352	3.200

Figure S3. EDS spectrum of the CF@Pt and the corresponding element ratio.

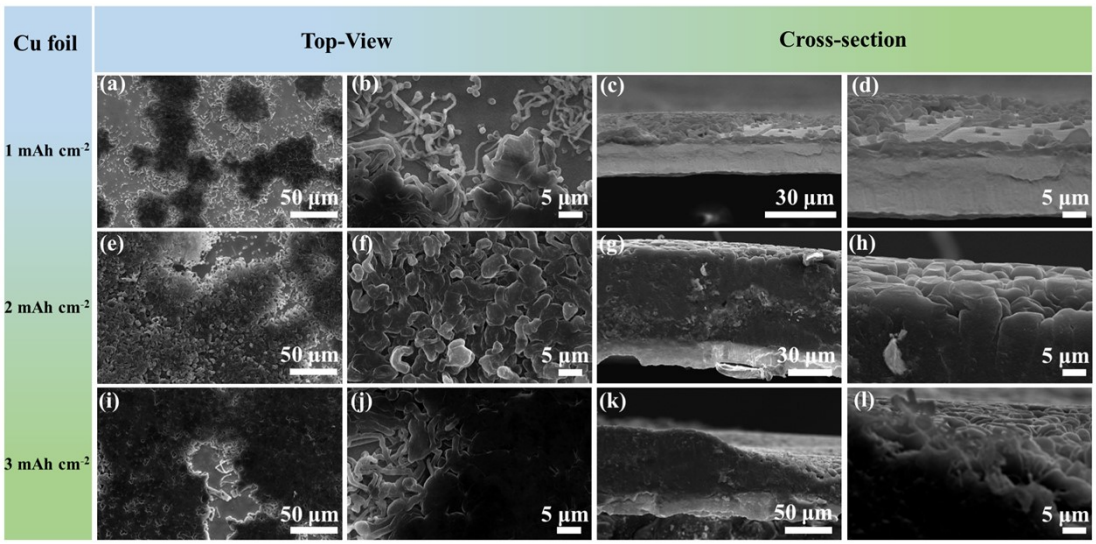

Figure S4. Top-views and cross-sectional SEM images of the Cu foil eletrode after plating (a-d) 1 mAh cm^{-2}, (e-h) 2 mAh cm^{-2} and (i-l) 3 mAh cm^{-2} at 0.5 mA cm^{-2}.

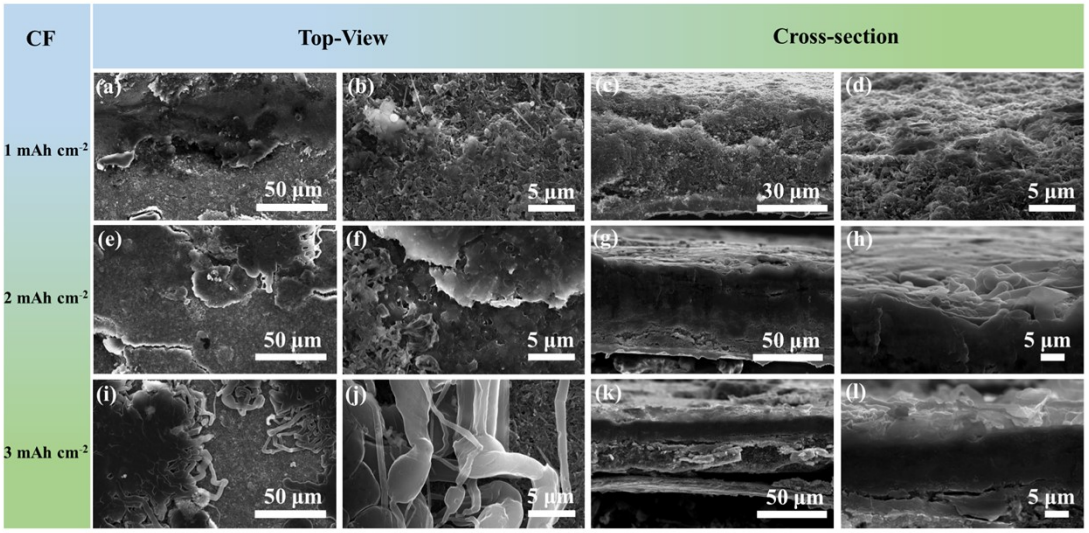

Figure S5. Top-views and cross-sectional SEM images of the CF eletrode after plating (a-d) 1 mAh cm^{-2}, (e-h) 2 mAh cm^{-2} and (i-l) 3 mAh cm^{-2} at 0.5 mA cm^{-2}.

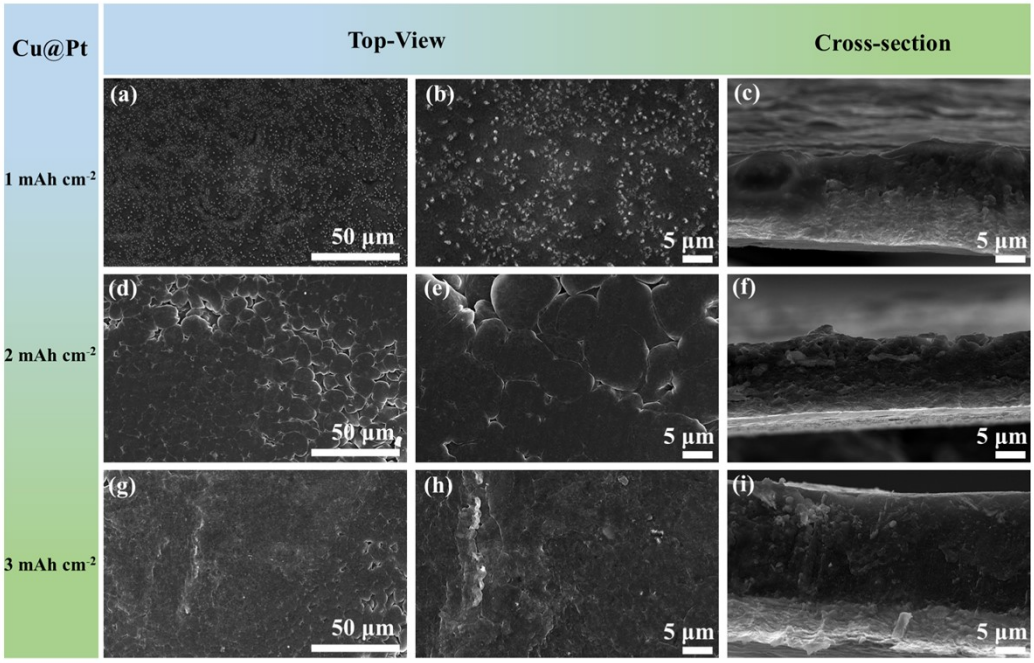

Figure S6. Top-view and cross-sectional SEM images of the Cu@Pt electrode after plating (a-c) 1 mAh cm^{-2}, (d-f) 2 mAh cm^{-2} and (g-i) 3 mAh cm^{-2} at 0.5 mA cm^{-2}.

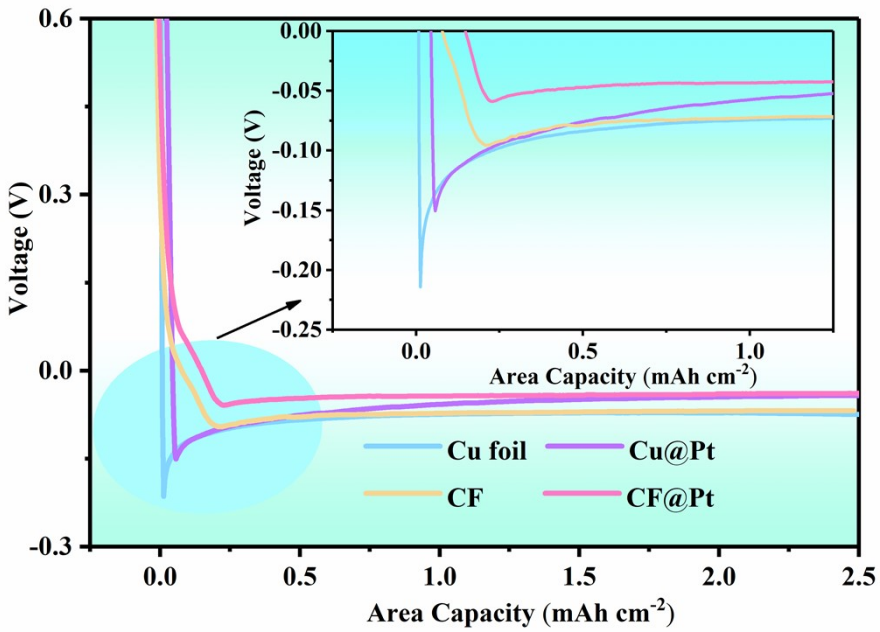

Figure S7. Plots of the nucleation overpotential of Li plating on the bare Cu foil, Cu@Pt, CF and CF@Pt electrodes at 0.5 mA cm^{-2} during the 1st plating/stripping process. The inset shows the enlarged plots of the nucleation overpotential.

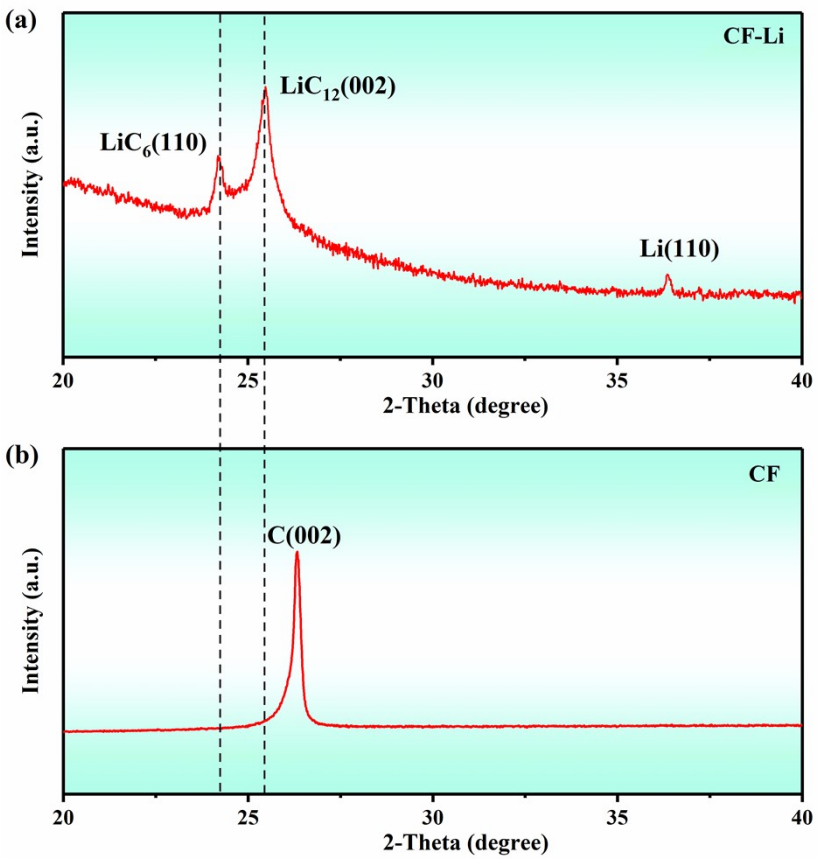

Figure S8. XRD patterns of (a) the charged CF electrode (charging with 1 mAh cm^{-2} of Li capacity) and (b) the pristine CF electrode.

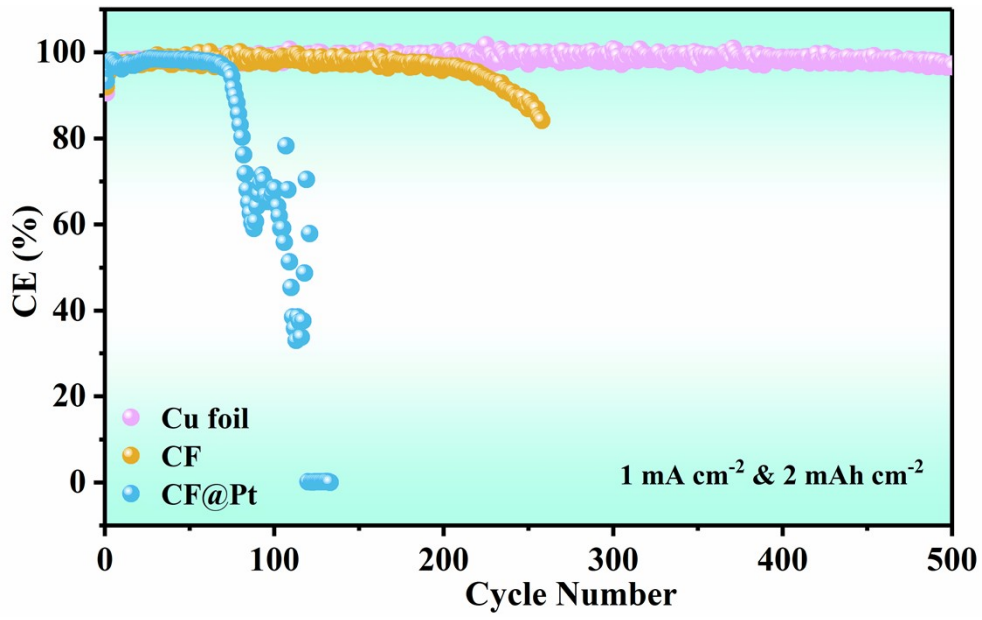

Figure S9. Comparison of Coulombic efficiency of the CF@Pt, CF, and Cu foil electrodes at 1 mA

cm^{-2} with a fixed capacity of 2 mAh cm^{-2}.

3. Electrochemical Performance Comparison

Table S1. Electrochemical performance comparison among recently reported host materials.

Host	Current ($mA\ cm^{-2}$)	Capacity ($mAh\ cm^{-2}$)	Cycle life	Average CE value	Ref.
Gradient-pore-size carbon skeleton (GPCS)	0.5	1	320 cycles	~98%	S1
Co-N-CNT-CF	0.5	1	200 cycles	98.4 %	S2
TiN/CNT scaffold	0.5	0.5	350 cycles	97.6%	S3
3-D carbon materials (CMs)	1	1	70 cycles	>97%	S4
Amide-functionalized carbon nanotube skeleton (A_f-CNT)	1	1	300 cycles	~ 97.8%	S5
Carbon fibers modified with ZnO (CFs@GZnO)	1	1	140 cycles	93.7 %	S6
GO-Zn/Cu	0.5	0.5	130 cycles	98%	S7
	1	2	110 cycles	96%	
Urchin-like Ag@CuO	0.5	1	550 cycles	98.86%	S8
rGO-Ag-S-CNT host	0.5	2	200 cycles	98.1%	S9
	1	2	90 cycles	97.9%	
SnS_2 nanosheet/carbon foam (SnS_2 NSA@CF)	1	1	400 cycles	~98%	S10
	3	1	280 cycles	98%	
Ni_2P/interconnected stacked hollow carbon	1	1	250 cycles	98.4%	S11
	3	1	226 cycles	98.1%	

spheres (Ni_2P@ISHCP)					
CF@Pt	0.5	1	800 cycles	98.73%	This
	1	1	700 cycles	98.62%	work
	2	1	380 cycles	98.01%	
	1	2	500 cycles	98.62%	

Table S2. Electrochemical performance comparison among recently reported host materials.

Host	Current ($mA\ cm^{-2}$)	Capacity ($mAh\ cm^{-2}$)	Overpotential (mV)	Cycle time (h)	Ref.
CFs@GZnO	1	1	24	400	S6
GO-Zn/Cu	1	1	20	620	S7
MXene@Au	1	1	~15	650	S12
N, O co-doped carbon nanosphere	1	1	28.8	560	S13
Porous CoP derived framework	1	1	/	350	S14
MnO@biomass-derived carbon nanofiber host	1	1	/	500	S15
$Li_{4.4}Sn$/SG	0.5	1	18	1000	S16
	1	1	34	600	
Silver-coated N-doped onion-like carbon spheres (Ag@NCS)	1	1	/	300	S17
ZnO@C-	2	1	28	320	S18

MWCNTs					
Carbon nanofibers with bidirectional gradient modification	1	1	39	630	S19
CF@Pt	0.5	1	13	1100	This
	1	1	19	770	work

Supplementary References:

S1. H. Liu, J. Di, P. Wang, R. Gao, H. Tian, P. Ren, Q. Yuan, W. Huang, R. Liu, Q. Liu and M. Feng, A novel design of 3D carbon host for stable lithium metal anode, *Carbon Energy*, 2022, **4**, 654-664.

S2. T. Lyu, F. Luo, Z. Wang, F. Jiang, S. Geng, Y. Zhuang, X. Lin, J. Chen, D. Wang, L. Bu, L. Tao, L. Liang and Z. Zheng, Bifunctional lithiophilic carbon fibers with hierarchical structure for high-energy lithium metal batteries, *Chemical Engineering Journal*, 2023, **466**, 143357.

S3. K. Yang, Y. He, Z. Gao, C. Li, F. Zhao, X. Xu, J. Li and X. Liu, Constructing a TiN/CNT lithiophilic scaffold for dendrite-free Li-metal anode, *Carbon*, 2024, **222**, 118999.

S4. Y. Xu, L. Wang, W. Jia, Y. Yu, R. Zhang, T. Li, X. Fu, X. Niu, J. Li and Y. Kang, Three-dimensional carbon material as stable host for dendrite-free lithium metal anodes, *Electrochimica Acta*, 2019, **301**, 251-257.

S5. G. Wang, T. Liu, X. Fu, Z. Wu, M. Liu and X. Xiong, Lithiophilic amide-functionalized carbon nanotube skeleton for dendrite-free lithium metal anodes, *Chemical Engineering*

Journal, 2021, **414**, 128698.

S6. Z. Xiao, D. Han, Y. Fu, K. Xie, W. Tian, C. Shu, K. Xi, C. Peng, Y. Wu, S. Dou and W. Tang, Eliminating concentration polarization with gradient lithiophilic sites towards high performance lithium metal anodes under low N/P ratio, *Chemical Engineering Journal*, 2024, **480**, 148029.

S7. J. Ma, J. Yang, C. Wu, M. Huang, J. Zhu, W. Zeng, L. Li, P. Li, X. Zhao, F. Qiao, Z. Zhang, D. He and S. Mu, Stabilizing nucleation seeds in Li metal anode via ion-selective graphene oxide interfaces, *Energy Storage Materials*, 2023, **56**, 572-581.

S8. M. Gao, Q. Dong, M. Yao, X. Wang, J. Li, W. Zhang, H. Huang, H. Guo, Z. Sun, Q. Chen, X. Han and W. Hu, Dual-gradient Engineering of Urchin-like Silver@Copper Oxide Heterostructures for Highly Stable Lithium Metal Anodes, *Advanced Functional Materials*, 2024, **34**, 2401442.

S9. X. L. Li, S. Huang, D. Yan, J. Zhang, D. Fang, Y. V. Lim, Y. Wang, T. C. Li, Y. Li, L. Guo and H. Y. Yang, Tuning Lithiophilicity and Stability of 3D Conductive Scaffold via Covalent Ag-S Bond for High-Performance Lithium Metal Anode, *Energy & Environmental Materials* 2023, **6**, e12274.

S10. D. Xie, H.-H. Li, W.-Y. Diao, R. Jiang, F.-Y. Tao, H.-Z. Sun, X.-L. Wu and J.-P. Zhang, Spatial confinement of vertical arrays of lithiophilic SnS2 nanosheets enables conformal Li nucleation/growth towards dendrite-free Li metal anode, *Energy Storage Materials*, 2021, **36**, 504-513.

S11. H. Jiang, Y. Zhou, H. Zhu, F. Qin, Z. Han, M. Bai, J. Yang, J. Li, B. Hong and Y. Lai, Interconnected stacked hollow carbon spheres uniformly embedded with Ni_2P

nanoparticles as scalable host for practical Li metal anode, *Chemical Engineering Journal*, 2022, **428**, 132648.

S12. Y. Qian, C. Wei, Y. Tian, B. Xi, S. Xiong, J. Feng and Y. Qian, Constructing ultrafine lithiophilic layer on MXene paper by sputtering for stable and flexible 3D lithium metal anode, *Chemical Engineering Journal*, 2021, **421**, 129685.

S13. C. Gao, J. Li, K. Sun, H. Li, B. Hong, M. Bai, K. Zhang, Z. Zhang and Y. Lai, Controllable lithium deposition behavior hollow of N, O co-doped carbon nanospheres for practical lithium metal batteries, *Chemical Engineering Journal*, 2021, **412**, 128721.

S14. X. Cao, Q. Wang, H. Wang, Z. Shang, J. Qin, W. Liu, H. Zhou and X. Sun, A mixed ion-electron conducting network derived from a porous CoP film for stable lithium metal anodes, *Materials Chemistry Frontiers*, 2021, **5**, 5486-5496.

S15. X. Chen, Z. Yuan, J. He, L. Tong, Y. Wang, J. Wu, X. Li and Y. Chen, A lithiophilic MnO@biomass-derived carbon nanofiber host for stable lithium-metal batteries, *Composites Communications*, 2023, **42**, 101660.

S16. Y. Jiang, J. Jiang, Z. Wang, M. Han, X. Liu, J. Yi, B. Zhao, X. Sun and J. Zhang, Li4.4Sn encapsulated in hollow graphene spheres for stable Li metal anodes without dendrite formation for long cycle-life of lithium batteries, *Nano Energy*, 2020, **70**, 104504.

S17. Z. Jiang, C. Meng, G. Chen, R. Yuan, A. Li, J. Zhou, X. Chen and H. Song, Lithiophilic onion-like carbon spheres as lithium metal uniform deposition host, *Journal of Colloid and Interface Science*, 2022, **627**, 783-792.

S18. W.-J. Yu, F. Liu, L. Zhang, Z. Liu, S. Wang and H. Tong, Lithiophilic ZnO confined in microscale carbon cubes as a stable host for lithium metal anodes, *Carbon*, 2022, **196**, 92-

101.

S19. T. Li, S. Gu, L. Chen, L. Zhang, X. Qin, Z. Huang, Y.-B. He, W. Lv and F. Kang, Bidirectional Lithiophilic Gradients Modification of Ultralight 3D Carbon Nanofiber Host for Stable Lithium Metal Anode, *Small*, 2022, **18**, 2203273.